

# Supporting Information

## Chemical Fate of Oils on Indoor Surfaces: Ozonolysis and Peroxidation

Zilin Zhou,<sup>1\*†</sup> Leigh R. Crilley,<sup>2‡</sup> Jenna C. Ditto,<sup>1§</sup> Trevor C. VandenBoer<sup>2</sup> and Jonathan P. D. Abbatt<sup>1\*</sup>

<sup>1</sup> Department of Chemistry, University of Toronto, Toronto, Ontario M5S 3H6, Canada

<sup>2</sup> Department of Chemistry, York University, Toronto, Ontario M3J 1P3, Canada

\* Corresponding authors.

Email: [zilin.zhou@hc-sc.gc.ca](mailto:zilin.zhou@hc-sc.gc.ca) (Z. Zhou) and [jonathan.abbatt@utoronto.ca](mailto:jonathan.abbatt@utoronto.ca) (J. P. D. Abbatt)

<sup>†</sup> Present address: Health Canada, Ottawa, Ontario K1A 0K9, Canada

<sup>‡</sup> Present address: WSP Australia, Brisbane, Queensland 4006, Australia.

<sup>§</sup> Present address: Department of Energy, Environmental, and Chemical Engineering, Washington University in St. Louis, St. Louis, Missouri 63130, United States

*This 23-page document contains 3 sections, including 2 tables and 10 figures.*

## **Table of Contents**

### **1. Materials and Methods**

Chemicals and sampling equipment

NMR sample preparations, operating conditions and calculations

ESI-MS sample preparations and operating conditions

EPR sample preparations and operating conditions

### **2. Cafeteria Kitchen Measurements**

Table S1. Relative signal intensities in Figure 2.

Figure S1. Light irradiance spectrum of indoor light at the cafeteria kitchen.

### **3. Office Measurements**

Figure S2. UV-Vis absorption spectrum of the canola oil and light irradiance measurements.

Figure S3. Neutral loss scan (+) ESI-MS/MS spectrum of the analyte in Figure 3f.

Table S2. Possible ion identities and structures of the reactants and oxidation products.

Figure S4. <sup>1</sup>H NMR spectra of fresh and covered oil coatings placed by a south-facing window.

Figure S5. Mechanism of lipid autoxidation and photosensitized oxidation (linoleate chains).

Figure S6. Full scan (-) ESI-MS spectrum of a dark covered oil coating by the window.

Figure S7. Full scan (-) ESI-MS spectra of unoxidized and photo-oxidized triolein coating.

Figure S8. Proposed mechanism of epoxide formation.

Figure S9. Proposed mechanism of secondary aldehyde formation.

Figure S10. Experimental EPR spectra of fresh and oxidized oil coatings.

### **References**

# 1. Materials and Methods

**Chemicals and sampling equipment.** Canola oil, which primarily contains triglycerides with oleate, linoleate, linolenate and saturated palmitate chains,<sup>1</sup> was purchased from a local retailer in Toronto, ON, Canada. Glyceryl tripalmitoleate ( $\geq 98\%$ , Sigma-Aldrich), triolein ( $\geq 99\%$ , Sigma-Aldrich), chloroform (Fisher Chemical), chloroform-D (Cambridge Isotope Laboratories), dimethyl sulfone (qNMR *TraceCERT* material, Sigma-Aldrich), 5,5-dimethyl-1-pyrroline *N*-oxide (also known as DMPO, TCI America), LC-MS grade ammonium formate ( $\text{NH}_4\text{HCOO}$ , Sigma-Aldrich), methanol (Fisher Chemical) and 2-propanol (Fisher Chemical) were used as received.

During sampling periods, indoor ozone was monitored by an ozone analyzer (Thermo Scientific Model 49i), and the relative humidity was monitored by a household hygrometer. Light irradiance at all sampling locations was measured by a spectral radiometer (StellarNet Inc). As well, the absorption spectrum of canola oil was measured using a UV-Vis spectrometer (Ocean Optics), with settings of 50 ms integration time and 100 average scans.

**NMR sample preparations, operating conditions and calculations.** As described in our previous study,<sup>2</sup> for all quantitative measurements ( $^1\text{H}$ -qNMR), each oil coating was extracted by 500  $\mu\text{L}$  0.45 mM dimethyl sulfone (internal standard) solution in  $\text{CDCl}_3$ . This extraction procedure provides sufficient signal-to-noise ratio (S/N) for key reagent and product signals in the spectra.<sup>2</sup> The extract was then transferred to a 3 mm NMR tube (Norell) for spectrum acquisition on an Agilent 600 MHz DD2 spectrometer. The major acquisition settings were: 9.6 kHz spectral width, 64 scans, 25 s relaxation delay, 4.5 s acquisition time and  $90^\circ$  pulse. Spectrum processing with phase correction and baseline correction (Bernstein polynomial fit) was applied. The signal of the solvent residual at 7.26 ppm was used as a reference for chemical shifts of all analyte signals. In the product yield analyses of the pre-deposited oil coatings, all peak integrals used in calculations were normalized to the integrated signal of  $\text{DMSO}_2$  internal standard at 3.0 ppm. Adapted from our previous study,<sup>2</sup> the degree of oxidation (DO) shown in eq. S1, was monitored through the decreasing signal intensity of the olefinic protons (signal **D** in Figure 2 or Table S1).

$$DO = 1 - \frac{I_{D(t)}}{I_{D(0)}} \text{ (eq. S1)}$$

where  $I_{D(0)}$ ,  $I_{D(t)}$  are the integrated signal **D** before and after indoor air exposure, respectively.

The secondary ozonide products after oxidation were characterized through the conversion of signal **D** (fresh oil) to the new signal **K** (aged oils). Based on the assumption that every carbon-carbon double bond in the triglycerides could be theoretically oxidized into SOZ, the molar yield was calculated through equation S2.

$$SOZ \text{ yield} = \frac{I_{K(t)}}{I_{D(0)}} \times \frac{1}{DO} \text{ (eq. S2)}$$

where  $I_{K(t)}$  is the integrated signal **K** measured in the oxidized sample.

The measurements obtained from the pre-deposited oil coatings were also used to estimate the thickness of organic films collected on clean surfaces. Here, it was assumed that aging did not alter the coating thickness. Besides, given that the relative integrals of glyceryl protons (**B**) remained constant during oxidation, the average thickness ( $l$ ) of the oil film deposited near the cooking area after 16 days was estimated through eq. S3.

$$l = \frac{I'_{B(t)}}{I_{B(0)}} \times 250 \text{ (nm)} \text{ (eq. S3)}$$

where  $I'_{B(t)}$  is the integrated signal **B** measured in the collected surface sample (clean Petri dish bottoms exposed to nearby cooking area after 16 days);  $I_{B(0)}$  is the integrated signal **B** measured in the pre-deposited canola oil coating whose average thickness is 250 nm.

For qualitative analyses without yield calculations, each oil coating was directly extracted by 500  $\mu$ L  $CDCl_3$ . The operating conditions were modified to increase signal-to-noise ratios and to shorten the measurement time: 9.6 kHz spectral width, 128 scans, 5 s relaxation delay, 4.5 s acquisition time and 90° pulse width. Spectrum processing followed the procedure mentioned above.

**ESI-MS sample preparations and operating conditions.** To complement the structural information from NMR spectra, samples were analyzed by direct infusion ESI-MS as a rapid and

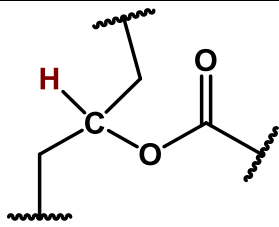
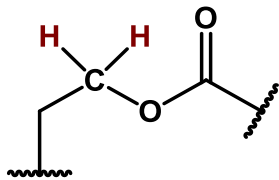
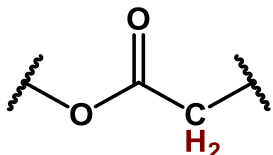
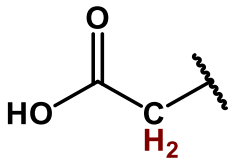
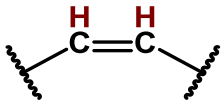
qualitative approach in product characterization.<sup>3-7</sup> Specifically, each oil coating was dissolved by 1 mL 0.25 mM glyceryl tripalmitoleate (internal standard) in 2-propanol, and was further diluted 10 times by 2 mM  $\text{NH}_4\text{HCOO}$  in methanol and 2-propanol mixture (60:40 v/v). This diluted analyte was then directly analyzed by a TSQ Endura Triple Quadrupole mass spectrometer (Thermo Scientific) with an ESI source at a sample infusion flow rate of  $10\ \mu\text{L}\ \text{min}^{-1}$ . Due to the presence of added salt, ammonium ( $[\text{M} + \text{NH}_4]^+$ ) and formate adducts ( $[\text{M} + \text{HCOO}]^-$ ) of the molecular ions were generated under positive and negative ion mode, respectively.<sup>3</sup> The typical full scan settings were as follows: 600-1200 m/z range, +3000 V (or -2200 V) spray voltage, 250°C ion transfer tubing temperature, 100°C vaporizer temperature and gas flows of  $\leq 25$ , 2, 0 (arbitrary units) for sheath gas, auxiliary gas and sweep gas, respectively.

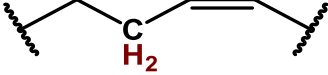
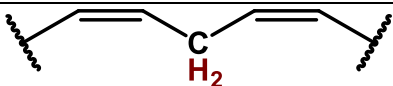
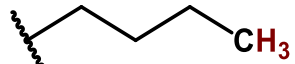
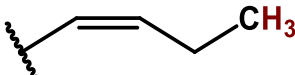
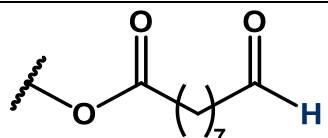
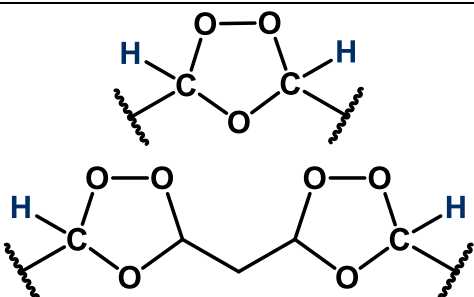
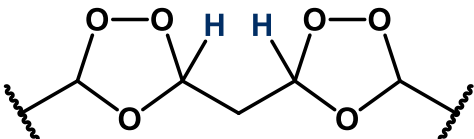
Previously, Zhou et al. developed a direct infusion tandem mass spectrometry (MS/MS) method for selectively detecting organic hydroperoxides (ROOH).<sup>8</sup> Here, to confirm the structure of such products, a similar neutral loss scan of 51 Da ( $\text{H}_2\text{O}_2 + \text{NH}_3$ ) of the ammoniated ions  $[\text{M} + \text{NH}_4]^+$  was implemented in (+)-ESI-MS/MS. With additional settings of 0.5 mTorr Argon pressure and collision-induced dissociation (CID) voltage of 20 V, all signals displayed in the spectrum are the selected precursor (ROOH) ions prior to fragmentation.

**EPR sample preparations and operating conditions.** Lastly, the organic radicals within the oil coatings were detected through a Bruker CW X-band ECS-EMXplus EPR Spectrometer. Here, each oil coating was extracted by 500  $\mu\text{L}$  chloroform containing DMPO spin trap ( $\sim 18\ \text{mM}$ ). Approximately 20  $\mu\text{L}$  of this mixed solution was immediately transferred to a sealed capillary tube prior to insertion into the EPR resonator (ER4123D). All recorded spectra were referenced to 2,2-diphenyl-1-picrylhydrazyl (DPPH). The primary EPR settings were: 9.34 GHz microwave frequency, 5.395 mW microwave power, 3331 G center field, 300.0 G sweep width, 50 dB receiver gain, 4 scans, 90 s sweep time, 30 ms conversion time, 0.01 ms time constant and 100 kHz modulation frequency with a modulation amplitude of 1. For radical speciation prediction, the experimental EPR spectrum was fitted through simulation by the SpinFit function in the Bruker Xenon software. The hyperfine splitting constants were calculated accordingly.

## 2. Cafeteria Kitchen Measurements

**Table S1.** (3 pages) Relative signal intensities in the  $^1\text{H}$  NMR spectra of fresh and aged oil coatings shown in Figure 2a-e. All peak integrals listed below are normalized to the dimethyl sulfone signal at 3.0 ppm. Sources of literature chemical shifts: Ref 2,9-13.

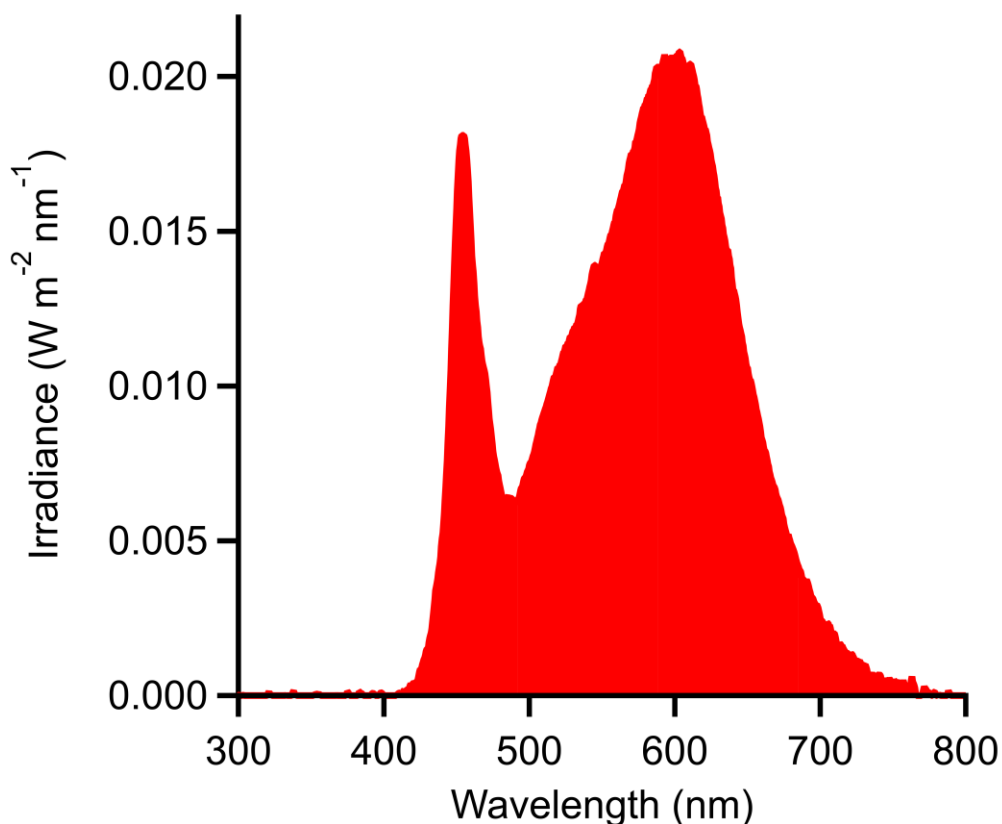
Chemical shift and assignment	Relative peak integral				
	(a) Fresh	(b) 2 days	(c) 6 days	(d) 9 days	(e) 16 days
 <b>A (glyceryl protons)</b> 5.26 ppm	0.43	0.44	0.41	0.46	0.42
 <b>B (glyceryl protons)</b> 4.14 and 4.29 ppm	0.85, 0.88	0.88, 0.91	0.82, 0.85	0.89, 0.93	0.84, 0.89
 2.27-2.34 ppm   2.33-2.37 ppm <b>C (<math>\alpha</math>-CH<sub>2</sub> to carbonyl, see note a)</b>	2.62	2.81	2.66	3.22	2.98
 <b>D (olefinic protons)</b> 5.29-5.43 ppm	3.19	2.52	1.36	0.66	0.30

 <b>E (allylic protons)</b> 1.96-2.11 ppm	4.73	4.05	2.53	1.41	0.68
 <b>F (bis-allylic protons)</b> 2.77 ppm – linoleate chains 2.80 ppm – linolenate chains	0.83	0.54	0.15	0	0
 <b>G (terminal methyl protons)</b> 0.88 ppm – saturated and oleate chains 0.89 ppm – linoleate chains	3.87	3.69	3.02	2.88	2.33
 <b>H (terminal methyl protons)</b> 0.97 ppm – linolenate chains	0.39	0.27	0.13	0	0
 <b>J (aldehydic protons)</b> 9.76 ppm	0	0.01	0.03	0.10	0.10
 <b>K (secondary ozonides)</b> 5.14 and 5.19 ppm	0	0.08, 0.06	0.10, 0.09	0.25, 0.23	0.24, 0.23
 <b>X (5.35-5.42 ppm, see note b)</b>	0	-	-	-	-

**Notes:**

[a] Signal **C** corresponds to methylene protons next to a carbonyl. This signal centers at 2.31 ppm for esters and 2.35 ppm for carboxylic acids.<sup>2</sup> In aged oil coatings, the slight increase in signal integrals was primarily seen in the peak associated with carboxylic acids, which are known ozonolysis products.

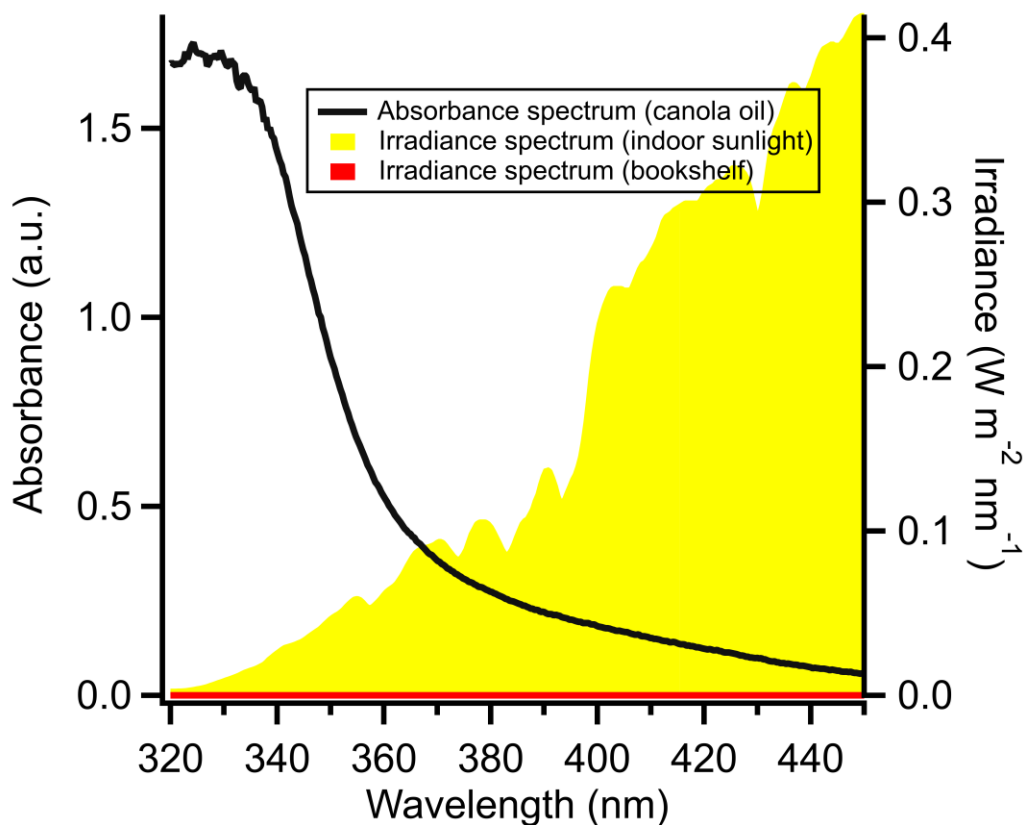
[b] Segal et al.<sup>12</sup> and de Oliveira et al.<sup>13</sup> propose that <sup>1</sup>H NMR signal associated with proton **X** shows distinct multiplets at 5.35-5.42 ppm. However, we did not observe this signal when the oil film was near full oxidation (Figure 2e). For this reason, only signal integration of **K** was used to calculate the molar yield of SOZs.



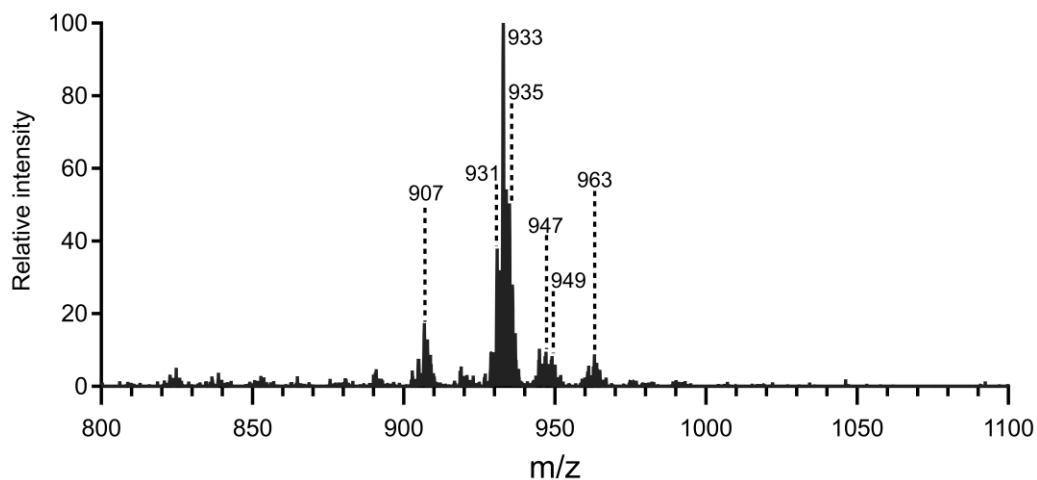
**Figure S1.** Measured irradiance spectrum of indoor light in the cafeteria kitchen (~2 m from the ceiling).



### 3. Office Measurements



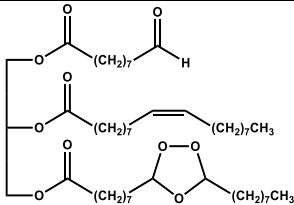
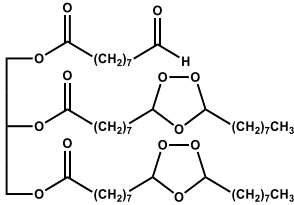
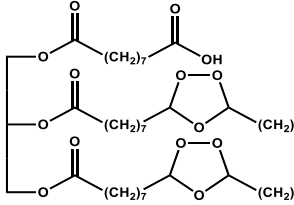
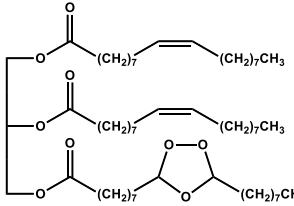
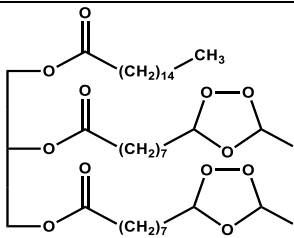
**Figure S2.** UV-Vis absorption spectrum (black line) of the canola oil used in this study and light irradiance measurements of two sampling locations. The irradiance spectra include the direct sunlight penetrating through a south-facing window along with indoor unshielded fluorescent lights (yellow shade) and light received on the bookshelf (red shade – at the very bottom of the figure) during the sampling period. Both spectra were measured in the early afternoon to represent the highest possible light intensity received at their respective sampling locations.

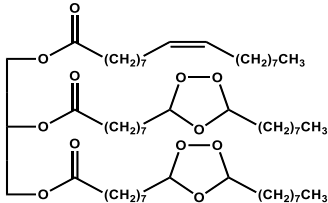
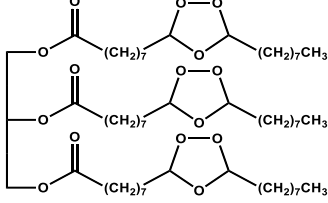
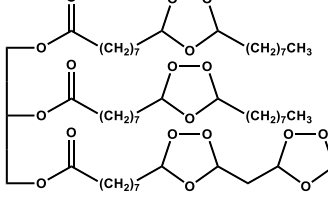


**Figure S3.** Neutral loss scan (+) ESI-MS/MS spectrum of the analyte in Figure 3f. The signals show the precursor ions whose fragmentation yields a neutral loss of 51 Da ( $\text{H}_2\text{O}_2 + \text{NH}_3$ ).<sup>8</sup> This fragmentation pattern is characteristic for ammoniated molecular ROOH ions. Thus, the major precursor ions (e.g.,  $m/z$  931-935 and 963) in the full scan spectrum (Figure 3f) were likely to be hydroperoxides. Note that there were additional signals ( $m/z$  947 and 949) in this figure that cannot be explained by the pattern of  $\Delta m/z = 32$ . More indoor sampling experiments were designed to monitor and characterize such products, which are explained in Section 3.3 of the article.

**Table S2.** (3 pages) Possible ion identities and structures of the major unsaturated triglycerides and oxidation products. Some structures are not explicitly shown due to the possibility of multiple isomers. The proposed secondary peroxidation products (i.e., epoxides) are not included.

MW	(+) m/z [M + NH <sub>4</sub> ] <sup>+</sup>	(-) m/z [M + HCOO] <sup>-</sup>	Proposed identity	Proposed structure (Isomers may be possible)
<b>Unsaturated triglycerides</b>				
801	819	846	TG(48:3) Glyceryl tripalmitoleate	
857	875	902	TG(52:3)	
859	877	904	TG(52:2)	
881	899	926	TG(54:5)	
883	901	928	TG(54:4)	
885	903	930	TG(54:3) Triolein	
<b>Oxidation products</b>				
775	/	820	[TG(54:3) – C <sub>9</sub> H <sub>18</sub> + O]	
791	/	836	[TG(54:3) – C <sub>9</sub> H <sub>18</sub> + 2O]	

823	841	/	[TG(54:3) – C <sub>9</sub> H <sub>18</sub> + 4O]	
871	889	/	[TG(54:3) – C <sub>9</sub> H <sub>18</sub> + 7O]	
887	/	932	[TG(54:3) – C <sub>9</sub> H <sub>18</sub> + 8O]	
889	907	/	[TG(52:3) + 2O]	TG(52:3) – OOH
913	931	958	[TG(54:5) + 2O]	TG(54:5) – OOH
915	933	960	[TG(54:4) + 2O]	TG(54:4) – OOH
917	935	962	[TG(54:3) + 2O]	TG(54:3) – OOH
931	949	/	[TG(54:4) + 3O]	TG(54:4) – SOZ
933	951	/	[TG(54:3) + 3O]	 TG(54:3) - SOZ
945	963	990	[TG(54:5) + 4O]	TG(54:5) - (OOH) <sub>2</sub>
955	973	/	[TG(52:2) + 6O]	 TG(54:2) - (SOZ) <sub>2</sub>
947	/	992	[TG(54:4) + 4O]	TG(54:4) - (OOH) <sub>2</sub>
977	/	1022	[TG(54:5) + 6O]	TG(54:5) - (OOH) <sub>3</sub>
979	997	/	[TG(54:4) + 6O]	TG(54:4) - (SOZ) <sub>2</sub>

981	999	/	[TG(54:3) + 6O]	 <p>TG(54:3) - (SOZ)<sub>2</sub></p>
1027	1045	/	[TG(54:4) + 9O]	TG(54:4) - (SOZ) <sub>3</sub>
1029	1047	/	[TG(54:3) + 9O]	 <p>TG(54:3) - (SOZ)<sub>3</sub></p>
1075	1093	/	[TG(54:4) + 12O]	 <p>TG(54:4) - (SOZ)<sub>4</sub></p>

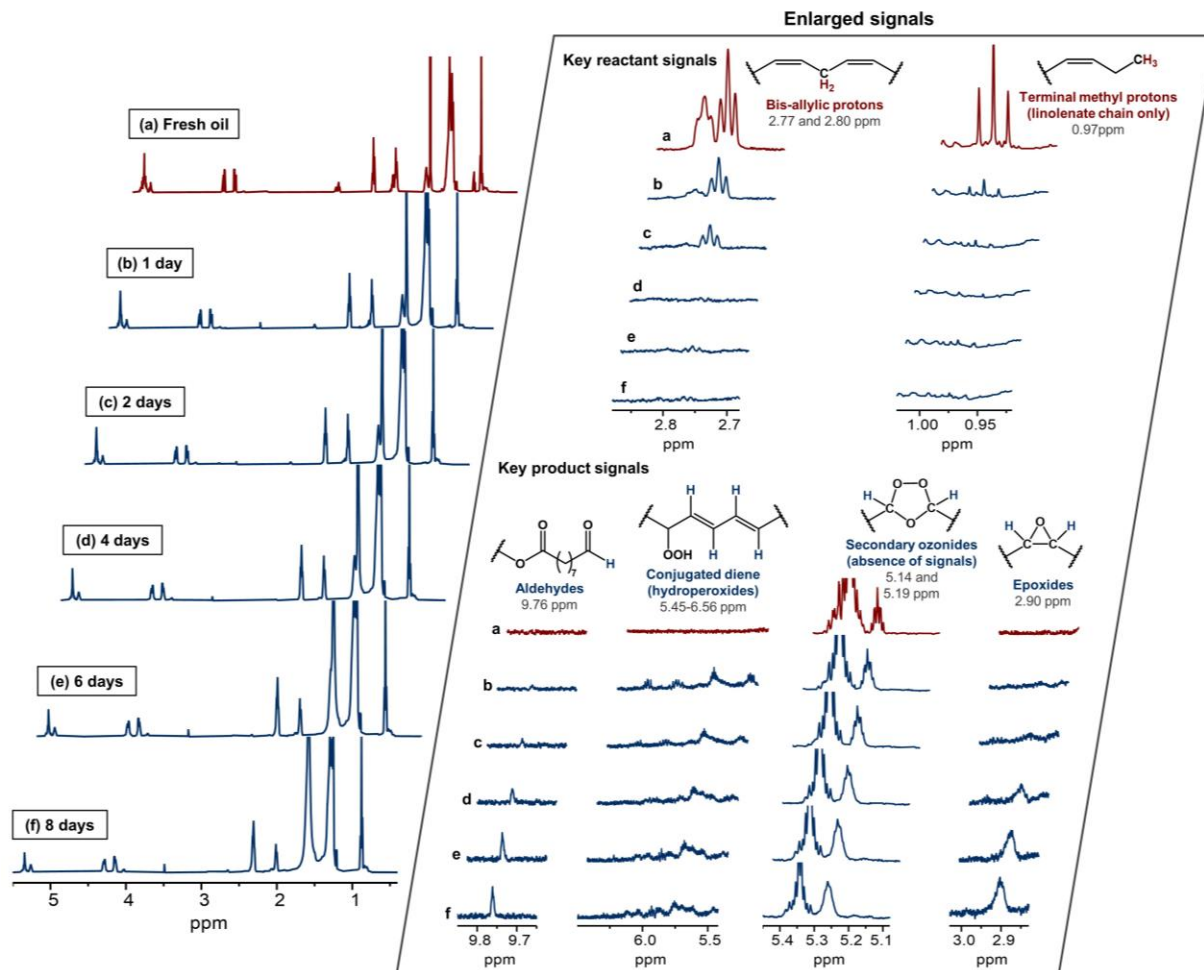


**Figure S4.** <sup>1</sup>H NMR spectra of (a) fresh canola oil coating and (b–f) covered oil coatings placed by a south-facing window after 1, 2, 4, 6 and 8 days. In the enlarged region, within 4 days, the degradation of unsaturated triglycerides could be seen through the consumption of bis-allylic hydrogens (2.77 and 2.80 ppm), and the terminal methyl protons associated with linolenate chains (0.97 ppm).<sup>9–13</sup> From the key product signals, no notable new peaks corresponding to secondary ozonides (5.14 and 5.19 ppm) were detected. Instead, weak proton signals of the conjugated diene associated with hydroperoxides appeared between 5.45 and 6.56 ppm. These light-sensitive peroxidation products were subject to further decomposition. In the late stage of exposure (4–8 days), signals demonstrating the new formation of condensed-phase aldehydes (9.76 ppm) and epoxides (2.90 ppm) were detected. These compounds were likely to be the secondary products accumulating on surfaces.<sup>11,14–18</sup> We do not attempt to quantify the peroxidation products due to weak signals and complex structures.

## Lipid autoxidation and photosensitized oxidation

Red arrows indicate the key steps

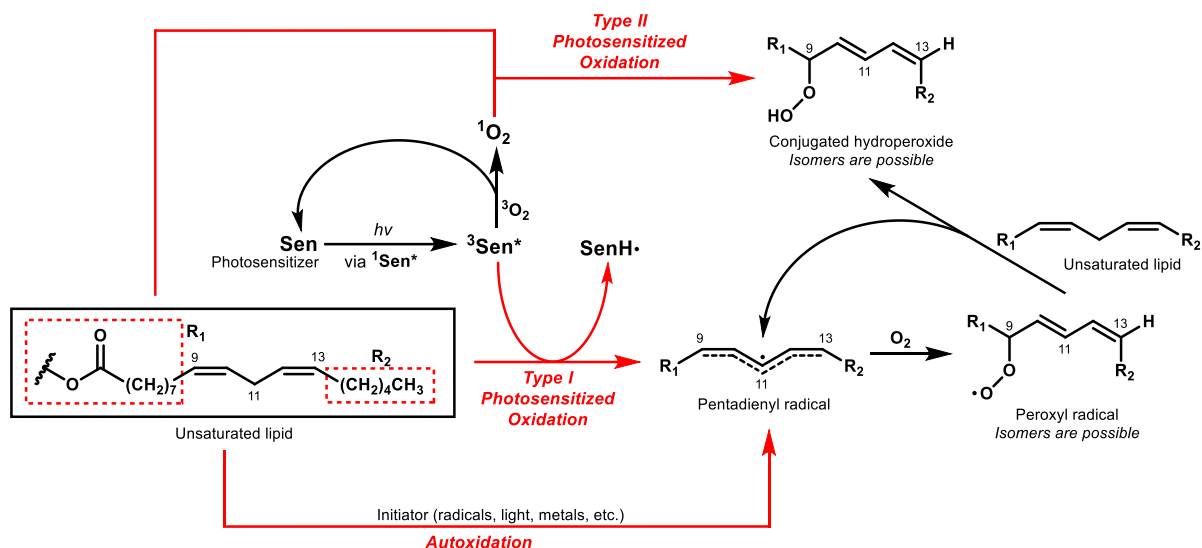


**Figure S5.** Mechanism of autoxidation and photosensitized oxidation of lipids containing linoleate chains.<sup>19-21</sup> In autoxidation, a pentadienyl radical moiety is formed after initiation. Molecular oxygen can be then added to C-9 (shown in figure), C-11 and C-13 of this delocalized radical, forming conjugated hydroperoxides (-OOH at C-9 and C-13) and non-conjugated hydroperoxides (-OOH at C-11). In the presence of light, the photosensitizer in plant oils absorbs photons to become an excited triplet species, after intersystem crossing from its excited singlet state. In Type I photosensitized oxidation, the excited triplet sensitizer abstracts a hydrogen atom from the unreacted lipid and generates hydroperoxides via the rest of the autoxidation mechanism. For Type II photosensitizers, the excited triplet sensitizer transfers the excess energy to triplet molecular oxygen. While the excited sensitizer returns to the ground state, the resulting singlet molecular oxygen reacts with oils to generate hydroperoxides.

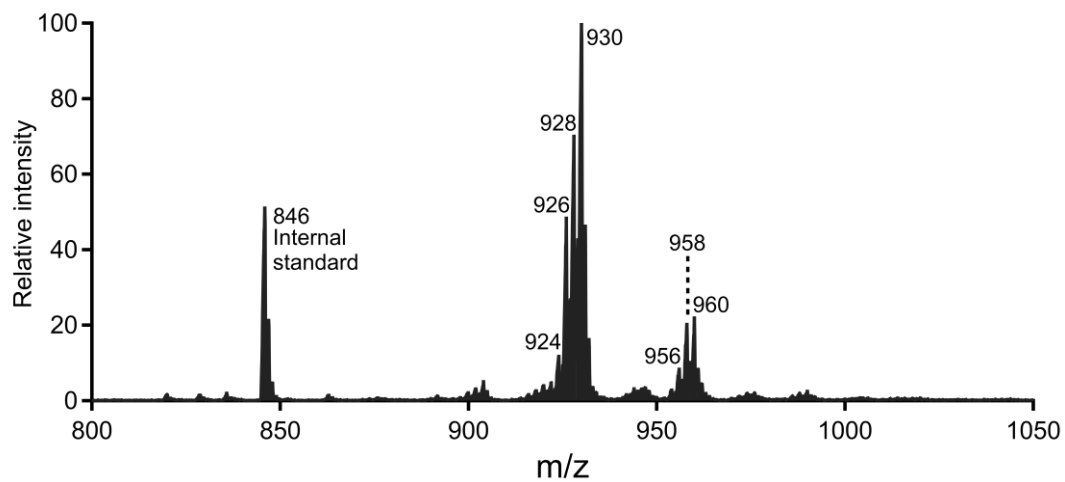


**Figure S6.** Full scan (-) ESI-MS spectrum of a covered oil coating after 4-day storage by the window. The glass Petri dish cover was fully wrapped with alumni foil during the aging process. This spectrum is very similar to that of the starting fresh oil, indicating the inactivity of oil film.



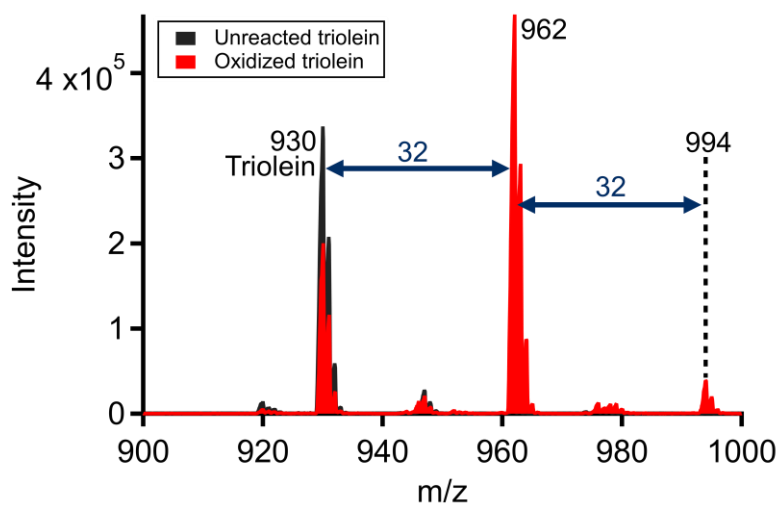


**Figure S7.** Full scan (-) ESI-MS spectra of an unoxidized (dark grey) and photo-oxidized triolein coating (red). The signal of the internal standard is not shown. The oxidation was done by placing a covered triolein coating by a south-facing window for 4 days. Given that pure triolein does not contain photosensitizers, direct sunlight by the window is sufficient to trigger peroxidation.

The diagram illustrates the formation of epoxides from unsaturated lipids via two pathways:

**Hydroperoxide-dependent pathway (top):**

- Hydrogen abstraction:** A Peroxyl radical (R<sub>1</sub>-CH(OO•)-CH=CH-CH=CH-R<sub>2</sub>) abstracts a hydrogen atom from an unsaturated lipid, forming a Hydroperoxide (R<sub>1</sub>-CH(OOH)-CH=CH-CH=CH-R<sub>2</sub>) and a pentadienyl radical (not shown).
- Decomposition:** The Hydroperoxide decomposes to form an Alkoxy radical (R<sub>1</sub>-CH(O•)-CH=CH-CH=CH-R<sub>2</sub>) and a hydroxyl radical (•OH).
- Rearrangement:** The Alkoxy radical undergoes a 1,5-hydrogen shift to form a new radical intermediate (R<sub>1</sub>-CH(O)-CH•-CH=CH-R<sub>2</sub>).
- Epoxide formation:** The intermediate reacts with H• to form the Epoxide (R<sub>1</sub>-CH(O)-CH(O)-CH=CH-R<sub>2</sub>).

**Hydroperoxide-independent pathway (bottom):**

- Peroxyl radical addition:** A Peroxyl radical (R<sub>1</sub>-CH(OO•)-CH=CH-CH=CH-R<sub>2</sub>) adds to the double bond of an unsaturated lipid, forming a cyclic peroxide intermediate (R<sub>1</sub>-CH(OO)-CH(OO)-CH=CH-R<sub>2</sub>).
- Intramolecular radical substitution:** The intermediate undergoes a 1,5-hydrogen shift to form an Alkoxy radical (R<sub>1</sub>-CH(O•)-CH=CH-CH=CH-R<sub>2</sub>).
- Epoxide formation:** The Alkoxy radical undergoes a 1,5-hydrogen shift to form the Epoxide (R<sub>1</sub>-CH(O)-CH(O)-CH=CH-R<sub>2</sub>).

**Unsaturated lipid structure:** The diagram shows a specific unsaturated lipid structure with a peroxide group (R<sub>1</sub>-CH(OO)-) and a double bond (CH=CH-CH=CH-R<sub>2</sub>), with carbon atoms numbered 9, 11, and 13. The structure is highlighted with a red dashed box.

S18

## Sources of secondary aldehydes and VOCs

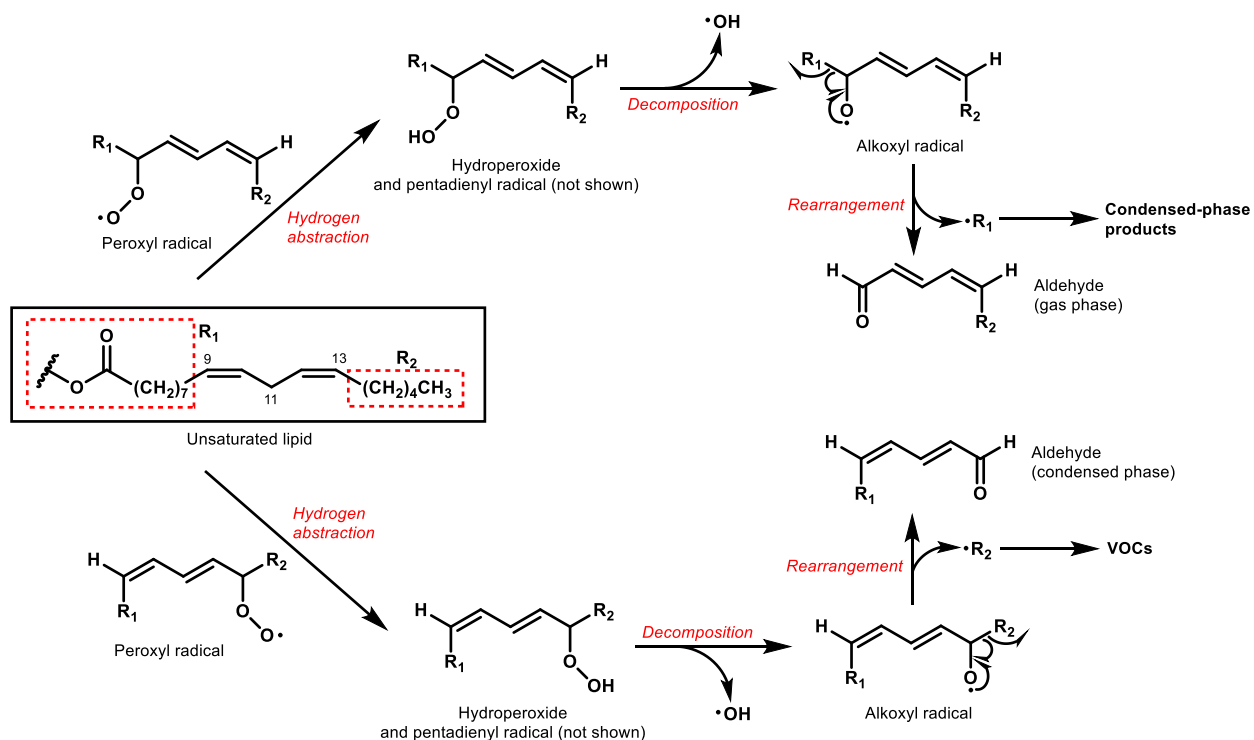


**Figure S9.** Proposed mechanism of secondary aldehyde formation.<sup>24</sup> Since  $R_1$  has much higher molecular weight than  $R_2$ , we assume that the products associated with these two groups are likely to be in the condensed phase and gas phase, respectively.

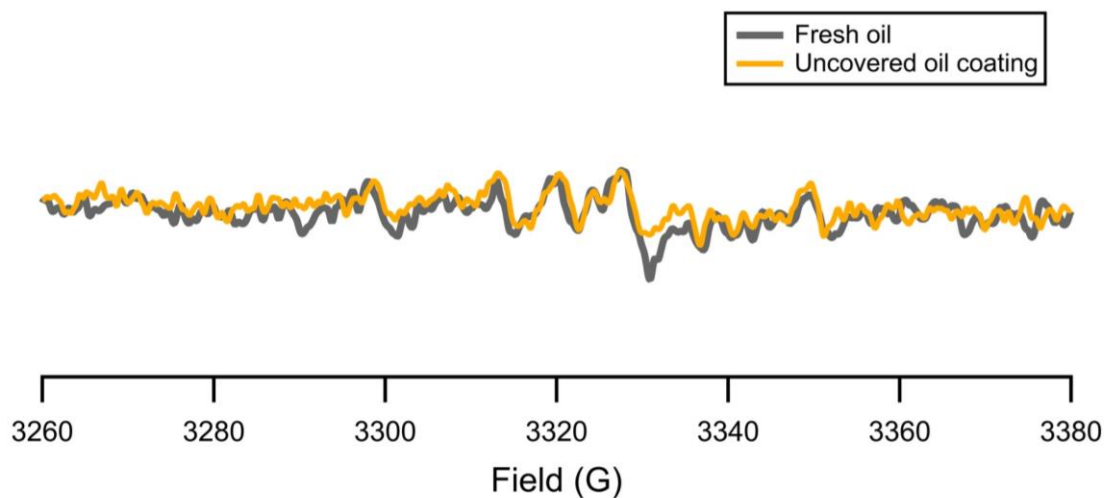


**Figure S10.** Experimental EPR spectra of fresh and oxidized oil coatings. The oxidation was done by placing the uncovered oil coating on a dark bookshelf for 3-day room air exposure. Under this condition, the oil coating was mostly oxidized by ozone. The EPR spectra indicate that oil ozonolysis is not a source of radicals. In contrast, significant radical formation was observed when the uncovered oil coating was placed by the window for 3 days (Figure 4g). Thus, we confirm that radicals found in the irradiated coating primarily originate from sunlight-initiated peroxidation which can occur simultaneously with ozonolysis.

## References

1. Andrikopoulos, N. K. Triglyceride species compositions of common edible vegetable oils and methods used for their identification and quantification. *Food Rev. Int.* **2002**, *18*, 71-102.
2. Zhou, Z.; Lakey, P. S. J.; von Domaros, M.; Wise, N.; Tobias, D. J.; Shiraiwa, M.; Abbatt, J. P. D. Multiphase Ozonolysis of Oleic Acid-Based Lipids: Quantitation of Major Products and Kinetic Multilayer Modeling. *Environ. Sci. Technol.* **2022**, *56*, 7716–7728.
3. Zhou, Z.; Zhou, S.; Abbatt, J. P. D. Kinetics and condensed-phase products in multiphase ozonolysis of an unsaturated triglyceride. *Environ. Sci. Technol.* **2019**, *53*, 12467-12475.
4. Li, M.; Butka, E.; Wang, X. Comprehensive quantification of triacylglycerols in soybean seeds by electrospray ionization mass spectrometry with multiple neutral loss scans. *Sci. Rep.* **2014**, *4*, 6581.
5. Catharino, R. R.; Haddad, R.; Cabrini, L. G.; Cunha, I. B. S.; Sawaya, A. C. H. F.; Eberlin, M. N. Characterization of vegetable oils by electrospray ionization mass spectrometry fingerprinting: classification, quality, adulteration, and aging. *Anal. Chem.* **2005**, *77*, 7429-7433.
6. Alves, J. O.; Botelho, B. G.; Sena, M. M.; Augusti, R. Electrospray ionization mass spectrometry and partial least squares discriminant analysis applied to the quality control of olive oil. *J. Mass Spectrom.* **2013**, *48*, 1109-1115.
7. Beneito-Cambra, M.; Moreno-González, D.; García-Reyes, J. F.; Bouza, M.; Gilbert-López, B.; Molina-Díaz, A. Direct analysis of olive oil and other vegetable oils by mass spectrometry: A review. *Trends Anal. Chem.* **2020**, *132*, 116046.
8. Zhou, S.; Rivera-Rios, J. C.; Keutsch, F. N.; Abbatt, J. P. D. Identification of organic hydroperoxides and peroxy acids using atmospheric pressure chemical ionization–tandem mass spectrometry (APCI-MS/MS): application to secondary organic aerosol. *Atmos. Meas. Technol.* **2018**, *11*, 3081-3089.
9. Soriano, N. U.; Migo, V. P.; Matsumura, M. Ozonation of sunflower oil: spectroscopic monitoring of the degree of unsaturation. *J. Am. Oil Chem. Soc.* **2003**, *80*, 997-1001.
10. Sadowska, J.; Johansson, B.; Johannessen, E.; Friman, R.; Broniarz-Press, L.; Rosenholm, J. B. Characterization of ozonated vegetable oils by spectroscopic and chromatographic methods. *Chem. Phys. Lipids* **2008**, *151*, 85-91.
11. Martínez-Yusta, A.; Goicoechea, E.; Guillén, M. D. A review of thermo-oxidative degradation of food lipids studied by <sup>1</sup>H NMR spectroscopy: influence of degradative conditions and food lipid nature. *Comp. Rev. Food Sci. Food Saf.* **2014**, *13*, 838-859.

12. Segal, A.; Zannardi, I.; Chiasserini, L.; Gabbriellini, A.; Bocci, V.; Travagli, V. Properties of sesame oil by detailed  $^1\text{H}$  and  $^{13}\text{C}$  NMR assignments before and after ozonation and their correlation with iodine value, peroxide value, and viscosity measurements. *Chem. Phys. Lipids* **2010**, *163*, 148-156.
13. de Oliveira, P.; De Almeida, N.; Conda-Sheridan, M.; Aparecido, R. do P.; Micheletti, A. C.; Carvalho, N. C.; dos Santos, E. d. A.; Marques, M. R.; de Arruda, E.; Alcantara, G. B.; de Oliveira, L. C.; de Lima, D.; Beatriz, A. Ozonolysis of neem oil: preparation and characterization of potent antibacterial agents against multidrug resistant bacterial strains. *RSC Adv.* **2017**, *7*, 34356–34365.
14. Guillén, M. D.; Ruiz, A. Monitoring of heat-induced degradation of edible oils by proton NMR. *Eur. J. Lipid Sci. Technol.* **2008**, *110*, 52-60.
15. Goicoechea, E.; Guillen, M. D. Analysis of hydroperoxides, aldehydes and epoxides by  $^1\text{H}$  nuclear magnetic resonance in sunflower oil oxidized at 70 and 100 °C. *J. Agric. Food Chem.* **2010**, *58*, 6234-6245.
16. Guillén, M. D.; Goicoechea, E. Detection of primary and secondary oxidation products by Fourier transform infrared spectroscopy (FTIR) and  $^1\text{H}$  nuclear magnetic resonance (NMR) in sunflower oil during storage. *J. Agric. Food Chem.* **2007**, *55*, 10729-10736.
17. Guillen, M. D.; Goicoechea, E. Oxidation of corn oil at room temperature: Primary and secondary oxidation products and determination of their concentration in the oil liquid matrix from  $^1\text{H}$  nuclear magnetic resonance data. *Food Chem.* **2009**, *116*, 183-192.
18. Xia, W.; Budge, S. M.; Lumsden, M. D. New  $^1\text{H}$  NMR-based technique to determine epoxide concentrations in oxidized oil. *J. Agric. Food Chem.* **2015**, *63*, 5780-5786.
19. Choe, E.; Min, D. B. Mechanisms and factors for edible oil oxidation. *Comp. Rev. Food Sci. Food Saf.* **2006**, *5*, 169-186.
20. Echegaray, N.; Pateiro, M.; Nieto, G.; Rosmini, M. R.; Munekata, P. E. S.; Sosa-Morales, M. E.; Lorenzo, J. M. Lipid oxidation of vegetable oils. In *Food Lipids*; Elsevier, 2022; pp 127–152.
21. Yin, H.; Xu, L.; Porter, N. A. Free radical lipid peroxidation: mechanisms and analysis. *Chem. Rev.* **2011**, *111*, 5944-5972.
22. Schaich, K. M. Thinking outside the classical chain reaction box of lipid oxidation. *Lipid Technol.* **2012**, *24*, 55-58.
23. Grüneis, V.; Fruehwirth, S.; Zehl, M.; Ortner, J.; Schamann, A.; König, J.; Pignitter, M. Simultaneous analysis of epoxidized and hydroperoxidized triacylglycerols in canola oil and margarine by LC-MS. *J. Agric. Food Chem.* **2019**, *67*, 10174-10184.

24. Choe, E.; Min, D. B. Chemistry of deep-fat frying oils. *J. Food Sci.* **2007**, 72, R77-R86.